



# Modeling the effect of light generation and light attenuation properties on the performance of phosphors used in medical imaging radiation detectors

I. Kandarakis, D. Cavouras\*

*Department of Medical Instrumentation Technology, Technological Educational Institution of Athens, Ag. Spyridonos Street, Aigaleo, 122 10 Athens, Greece*

Received 8 March 2000; received in revised form 1 August 2000; accepted 31 August 2000

## Abstract

A theoretical description of the effect of light generation and light attenuation properties on the imaging performance of phosphor materials used in radiation detectors of medical imaging systems is presented. The description is based on a theoretical model employing analytical expressions for the detector optical gain (DOG) (emitted optical quanta per incident X-ray), the modulation transfer function (MTF), and the detective quantum efficiency (DQE) as functions of optical properties of phosphors. The model was used to fit experimental DOG-data and to estimate the values of two important parameters: (1) the intrinsic X-ray to light conversion efficiency, expressing the property of light generation within the phosphor material; (2) the reciprocal diffusion length, expressing the property of light attenuation within the phosphor material. For this study,  $\text{La}_2\text{O}_2\text{S:Tb}$ ,  $\text{Y}_2\text{O}_2\text{S:Tb}$ ,  $\text{Y}_2\text{O}_2\text{S:Eu}$ , and  $\text{Y}_2\text{O}_3:\text{Eu}$  phosphor materials were employed. Additionally, the sensitivity of DOG, MTF, and DQE on the variation of the intrinsic X-ray to light conversion efficiency and of the optical attenuation coefficient within the phosphor was theoretically studied. It was found that (1) DOG increases with increasing intrinsic X-ray to light conversion efficiency and decreases with increasing optical attenuation coefficient; (2) MTF increases with increasing optical attenuation while it remains unaltered by varying the intrinsic X-ray to light conversion efficiency and (3) DQE decreases with increasing optical attenuation and remains constant with increasing X-ray to light conversion efficiency. © 2001 Elsevier Science B.V. All rights reserved.

*Keywords:* Phosphor screens; Scintillators, MTF; DQE

## 1. Introduction

Phosphors are materials that emit optical quanta when excited by X-rays or other types of radiation. Phosphor layers (screens) combined with optical

sensors (films, photocathodes, and photodiodes) are used in radiation detectors of medical imaging systems. The performance of the latter is usually assessed by determining various image quality metrics, which express image brightness, spatial resolution, image contrast and noise. These properties depend strongly on the intrinsic physical properties of the phosphor materials and on the energy of the incident radiation quanta.

In the present study a theoretical description of the imaging performance of phosphors is developed based on optical properties, which are derived from

\* Correspondence address: 37-39 Esperidon Street, Kallithea 17671, Athens, Greece. Tel: + 30-1-5385-375 or + 30-1-5385-372; fax: + 30-1-5910-975.

*E-mail addresses:* cavouras@hol.gr, cavouras@ee.teiath.gr (D. Cavouras).

experimental data. The purpose is to examine the influence of light generation and light attenuation properties on the overall phosphor performance. The study was accomplished by the determination of the following image quality metrics:

1. The detector optical gain (DOG), which is defined as the number of emitted optical photons (NEP) per incident X-ray quantum [1,2]. DOG is directly related to the image brightness that can be achieved for a given level of radiation fluence incident on the phosphor. Additionally, DOG may be expressed as a function of spatial frequency. In this case DOG is equivalent to the contrast transfer function (CTF) usually defined for films and screen-film systems used in medical radiography [3].
2. The modulation transfer function (MTF) which expresses image contrast and spatial resolution in the spatial frequency domain [4,5]. MTF may be defined in terms of the Fourier transform of the point spread function (PSF). PSF expresses light spread due to isotropic light emission and optical scattering within the phosphor material and describes the spatial distribution of the optical quanta originating from a point source.
3. The detective quantum efficiency (DQE) that expresses the efficiency of an imaging system to transfer the signal-to-noise ratio (SNR) from the input to its output [6–8]. DQE is a function of the spatial-frequency-dependent DOG and of the noise power spectrum (NPS), also called the Wiener spectrum [6,9,10]. NPS describes image noise in the spatial frequency domain.

Using the formulation proposed in this study the imaging performance of a phosphor may be predicted, provided that a number of optical parameters, namely, the intrinsic X-ray to light conversion efficiency (light generation properties) and the coefficients related to optical attenuation (scattering, absorption), are obtained from experimental measurements. In this study DOG, MTF, and DQE were calculated for various values of the aforementioned optical parameters in order to examine the effect of those parameters on phosphor performance.

## 2. Material and methods

### 2.1. Theory

Consider an X-ray quantum fluence  $\Phi_Q$  (X-ray quanta/unit of area) incident on the surface of the phosphor layer of an X-ray imaging detector. A fraction  $\eta_Q$  of these X-ray quanta will interact with the phosphor mass and will cause the emission of optical quantum fluence  $\Phi_\lambda$  (optical quanta/unit of area). Considering mean values for  $\Phi_Q$ ,  $\eta_Q$ , and  $\Phi_\lambda$ , averaged over the whole detector area, the emitted optical quantum fluence may be written as follows:

$$\bar{\Phi}_\lambda(E, \hbar\omega, w) = \bar{\Phi}_Q(E)\bar{\eta}_Q(E, w)\bar{m}_0(E, \hbar\omega)\bar{g}_\lambda(s, a, w) \quad (1)$$

where  $E$  is the energy of an X-ray quantum,  $\omega$  is the frequency of optical quanta and, thus,  $\hbar\omega$  denotes the energy of an optical quantum,  $w$  is the coating weight of the phosphor layer (screen) (in  $\text{mg}/\text{cm}^2$ ),  $\bar{m}_0$  is the mean number of optical quanta created within the phosphor per interacting X-ray quantum,  $\bar{g}_\lambda$  is the mean fraction of generated optical quanta that escape from the non-irradiated phosphor surface,  $a$  and  $s$  are coefficients of optical absorption and optical scattering, respectively, characterizing the phosphor material.  $\eta_Q$  and  $g_\lambda$  are the quantum detection efficiency (QDE) and light transmission efficiency (LTE), respectively [2,11,12].

If the incident X-ray beam is polyenergetic, relation (1) must be integrated over the X-ray spectrum.

$$\bar{\Phi}_\lambda(E_0, \hbar\omega, w)$$

$$= \int_0^{E_0} \bar{\Phi}_Q(E)\bar{\eta}_Q(E, w)\bar{m}_0(E, \hbar\omega)\bar{g}_\lambda(s, a, w) dE \quad (2)$$

where  $E_0$  is the maximum energy of the spectrum, which is numerically equal to the X-ray tube voltage.

$\bar{\Phi}_\lambda$  may be determined by calculating the four quantities in the integral of formula (2) as follows:

1.  $\Phi_Q(E)$  may be simulated by the theoretical model for X-ray spectra developed by Tucker

et al. (1991) [13]:

$$\Phi_Q(E) = \left[ \frac{\alpha r_e Z^2}{AE} \right] \int_E^{E_0} \left[ \frac{B}{E_e} \right] [E_0 + m_e c^2] \times f_T(E, E_0) \left[ \frac{1}{\rho} \frac{dE_e}{dx} \right] dE_e \quad (3a)$$

where  $\alpha$  is the fine structure constant,  $r_e$  is the classical electron radius,  $Z$  is the atomic number of the target material (X-ray tube anode) – usually tungsten or molybdenum –  $A$  is the mass of the target atoms,  $E_0$  is the kinetic energy of the incident electron,  $E_e$  is the penetrating electron energy,  $m_e$  is the rest mass of an electron,  $c$  is the velocity of light,  $(1/\rho)[dE_e/dx]$  is the mass stopping power of the target material,  $f_T(E, E_0)$  is the fraction of X-ray quanta transmitted by the anode given by

$$f_T(E, E_0) = \frac{\exp[-\mu_A(E)(E_0^2 - E_e^2)]}{\rho_A c_{TW} \sin(\theta + \varphi)} \quad (3b)$$

where,  $\mu_A(E)$  and  $\rho_A$  is the linear attenuation coefficient and density of the anode material respectively,  $c_{TW}$  is the Thomson–Whiddington constant [13],  $\theta$  is the target angle,  $\varphi$  is the angle off the central axis along which an X-ray quantum travels,  $x$  is the depth of electron penetration within the target,  $B$  is a function of  $Z$  and  $T$  given by Tucker et al. [13]. Most data and functions necessary for  $\Phi_Q$  calculations were taken from Ref. [13] and from X-ray unit manufacturer's data.

2.  $\eta_Q$  may be approximated by considering exponential X-ray absorption [2], which is governed by the corresponding absorption coefficients and phosphor thickness (or coating weight). X-ray absorption coefficients for various materials may be calculated from data on chemical elements as tabulated by Storm and Israel [14].
3.  $m_0$  may be calculated by the formula:  $m_0 = \eta_c E / \hbar \omega$ .  $\eta_c$  is the intrinsic X-ray to light conversion efficiency, expressing the fraction of X-ray energy absorbed in the phosphor, which is converted into optical quanta energy (light).

For polychromatic optical emission spectra the mean optical quantum energy may be used

$$\langle \hbar \omega \rangle = \frac{\int \Phi_\lambda^N(\hbar \omega) \hbar \omega d\hbar \omega}{\int \Phi_\lambda^N(\hbar \omega) d\hbar \omega} \quad (3c)$$

where  $\Phi_\lambda^N$  is the normalized spectral distribution function of the emitted optical quanta.

4.  $g_\lambda$  may be calculated by the following formula:

$$\bar{g}_\lambda(a, s, w_0) = \int_0^{w_0} \phi_R(E, w) g_w(a, s, w) dw \quad (4)$$

where  $\phi_R$  is a probability distribution function describing the probability of an interacting X-ray quantum to be absorbed within an elementary thin layer  $dw$  at depth  $w$  and  $g_w$  is a function giving the fraction of optical quanta generated within the layer  $dw$  that escape to the phosphor output after transmission through a phosphor layer of coating weight  $(w_0 - w)$ ,  $w_0$  being the total coating weight of the layer. Relation (4) expresses the average fraction of emitted optical quanta (or average probability of optical emission) per X-ray quantum absorbed. Function  $\phi_R(E, w)$  may be expressed by the formula

$$\phi_R(E, w) = \frac{[\exp(-\mu(E)w)]\mu(E)dw}{\int_0^{w_0} [\exp(-\mu(E)w)]\mu(E)dw} \quad (5)$$

where  $\mu(E)$  is the X-ray absorption coefficient of the phosphor material. The numerator in Eq. (5) expresses the fraction of incident X-ray quanta absorbed in the thin layer  $dw$  at depth  $w$  while the denominator is the fraction absorbed within the whole layer  $w_0$ .

The function  $g_w$  may be calculated by expressing it in the spatial frequency domain in terms of the optical properties of the phosphor material (absorption, scattering etc.). This has been accomplished by solving a photon diffusion differential equation [4], resulting in

$$g_w(a, s, w) = \frac{\tau \rho_1 [(q + \tau \rho_0)e^{qw} + (q - \tau \rho_0)e^{-qw}]}{(q + \tau \rho_0)(q + \tau \rho_1)e^{qw_0} - (q - \tau \rho_0)(q - \tau \rho_1)e^{-qw_0}}, \quad (6)$$

where  $\tau$  is called the inverse relaxation length, which is inversely proportional to the mean optical absorption and mean transport free path lengths [2,4,10,12].  $\rho_0, \rho_1$  are parameters related to light reflectivities at front and back phosphor surfaces as follows:

$$\rho_i = \frac{1 - r_i}{1 + r_i}, \quad i = 0, 1 \quad (7a)$$

where  $r_0$  and  $r_1$  are the front and back light reflectivity coefficients,  $q$  in Eq. (6) is a parameter given by the relation

$$q = \left[ 4\pi^2 \left( \frac{u}{\rho_M} \right)^2 + \sigma^2 \right]^{1/2} \quad (7b)$$

where  $u$  is the spatial frequency,  $\sigma$  is the reciprocal diffusion length, and  $\rho_M$  is the phosphor material density.  $\sigma$  is an optical attenuation coefficient that may be expressed as a function of optical coefficients of absorption ( $a$ ) and scattering ( $s$ ):

$$\sigma = [a(a + 2s)]^{1/2} \quad (7c)$$

$\tau$  in Eq. (6) may be expressed [2,4,11] as

$$\tau = \frac{\sigma}{\beta} = \frac{\sigma}{(1 - R_\infty)/(1 + R_\infty)} \quad (7d)$$

where  $\beta$  is an optical parameter defined in terms of  $R_\infty$ , which is the front reflectivity ( $r_0$ ) corresponding to a very thick phosphor layer with no light transmission through it [11]. Thus, according to relations (6) and (7b),  $\Phi_\lambda$  may now be expressed in the spatial frequency domain [ $\Phi_\lambda(u, E, \hbar\omega, w)$ ].

$\Phi_\lambda$  depends on the level of the incident X-ray quantum fluence and, thus, it is not strictly related to the physical properties of the phosphor material. To describe the phosphor performance independent of the quantity of the incident radiation, the detector optical gain  $G_D$ , may be defined by the following expression:

$$G_D(u, w) = \frac{\bar{\Phi}_\lambda(u, E_0, \hbar\omega, w)}{\int_0^{E_0} \bar{\Phi}_Q(E) dE}. \quad (8)$$

The modulation transfer function  $M_P$  of a phosphor layer is obtained by normalizing the optical quantum fluence as follows:

$$M_P(u, w) = \frac{\bar{\Phi}_\lambda(u, E_0, \hbar\omega, w)}{\bar{\Phi}_\lambda(u = 0, E_0, \hbar\omega, w)} \\ = \frac{G_D(u, w) \int_0^{E_0} \bar{\Phi}_Q(E) dE}{G_D(0, w) \int_0^{E_0} \bar{\Phi}_Q(E) dE} = \frac{G_D(u, w)}{G_D(0, w)} \quad (9)$$

or

$$M_P(u, w) = \frac{G_D(u, w)}{G_D(0, w)}. \quad (10)$$

For  $u \neq 0$ ,  $G_D$  corresponds to the contrast transfer function (CTF) that has been previously defined for photographic or radiographic films and for radiographic screen-film systems [3,15].

$G_D$  and  $M_P$  are functions that describe the response of an image detector to an input signal. However, a complete description of the overall detector performance should also include the effects of quantum noise. The latter expresses the fluctuations in the number of emitted optical quanta throughout the phosphor emitting surface, for uniform X-ray irradiation. In the space domain, quantum noise is described by the variance in the number of emitted optical quanta per unit of area ( $\bar{\Phi}_\lambda$ ), while in the spatial frequency domain noise is expressed by the noise amplitude spectrum or by the noise power spectrum (Wiener spectrum) [6,15,16]. To include both the effects of signal ( $\bar{\Phi}_\lambda$ ) and noise (variance in  $\bar{\Phi}_\lambda$ ) in a single function, two parameters, the signal-to-noise ratio (SNR) and the detective quantum efficiency (DQE), have been defined [6–8,15]. DQE is a transfer function describing the efficiency of a detector to transfer SNR from the input (I) to the output (O), given by the ratio

$$DQE(u, w) = \left[ \frac{SNR_O}{SNR_I} \right]^2. \quad (11)$$

Considering that  $\Phi_\lambda(u, E_0, \hbar\omega, w)$  represents the output signal and denoting the noise amplitude

spectrum by  $N_Q(u, \Phi_Q, \hbar\omega, w)$  and using Eqs. (9) and (10),  $\text{SNR}_0^2$  may be written as

$$\begin{aligned} \text{SNR}_0^2 &= \frac{\bar{\Phi}_\lambda^2(u, E_0, \hbar\omega, w)}{N_Q^2(u, \Phi_Q, \hbar\omega, w)} \\ &= \frac{\left[ G_D(u, w) \int_0^{E_0} \Phi_Q(E) dE \right]^2}{W_Q(u, \Phi_Q, \hbar\omega, w)} \\ &= \frac{\left[ G_D(0, w) M_P(u, w) \int_0^{E_0} \bar{\Phi}_Q(E) dE \right]^2}{W_Q(u, \Phi_Q, \hbar\omega, w)}, \quad (12a) \end{aligned}$$

where  $W_Q$  is the noise power spectrum (Wiener) which is equal to  $N_Q^2$ . Considering that the input signal is represented by the mean incident X-ray quantum fluence  $\Phi_Q$  and the input quantum noise is represented by the variance in  $\Phi_Q$ ,  $\text{SNR}_1^2$  may be written as

$$\text{SNR}_1^2 = \frac{\bar{\Phi}_Q^2}{\text{var}[\Phi_Q]}. \quad (12b)$$

Assuming that the incident X-ray quanta follow Poisson statistics,

$$\text{var}[\Phi_Q] = \bar{\Phi}_Q \quad \text{and hence, } \text{SNR}_1^2 = \bar{\Phi}_Q.$$

Thus,

$$\text{DQE}(u, w) = \frac{\left[ G_D(u, w) \int_0^{E_0} \bar{\Phi}_Q(E) dE \right]^2}{W_Q(u, \Phi_Q, \hbar\omega, w) \int_0^{E_0} \bar{\Phi}_Q(E) dE} \quad (13)$$

or

$$\text{DQE}(u, w) = \frac{[G_D(0, w) M_P(u, w)]^2 \bar{\Phi}_Q}{W_Q(u, \Phi_Q, \hbar\omega, w)}. \quad (14)$$

It can be shown [10,16,17] that  $W_Q$  may be expressed as a function of  $\eta_Q, m_0$ , and  $g_\lambda$  by the following relation:

$$\begin{aligned} W_Q(\Phi_Q, u, \hbar\omega, w) &= \int_0^{E_0} \Phi_Q(E) \bar{\eta}_Q(E, w) \\ &\quad \times [\bar{m}_0(E, \hbar\omega) \bar{g}_\lambda(a, s, u, w)]^2 dE \\ &\quad + \int_0^{E_0} \Phi_Q(E) \bar{\eta}_Q(E, w) \bar{m}_0(E, \hbar\omega) \\ &\quad \times \bar{g}_\lambda(a, s, 0, w) dE. \quad (15) \end{aligned}$$

As it can be seen from relations (2), (4), (6), (8)–(10), (13), and (15) the values of  $G_D, M_P, W_Q$  and DQE depend on the same intrinsic physical parameters, namely  $\mu, \sigma, \tau, \rho_i, \eta_C$  which govern the response of a phosphor layer to an incident X-ray beam. If the values of the aforementioned parameters are known, the response of the phosphor may be theoretically predicted. An additional remark is that  $G_D$  is of primary importance in the evaluation of phosphor materials, since  $G_D$  affects the values of both MTF and DQE (see relations (9), (10), (13)).

## 2.2. Experiments and calculations

The suitability of the model to describe experimental data was tested on experimental data concerning  $G_D$ . Additionally, using the theoretical model, the influence of intrinsic parameters  $\sigma, \eta_C$ , and material density on  $G_D, M_P$ , and DQE was studied.

### 2.2.1. Detector optical gain ( $G_D$ ) determination

$G_D$  was experimentally determined by the following procedure [1,2,8,12,15,17]

1. Phosphor layers were prepared in the laboratory by the sedimentation of the phosphor in powder form on fused silica substrates. Powders of various phosphors ( $\text{La}_2\text{O}_2\text{S}:\text{Tb}$ ,  $\text{Y}_2\text{O}_2\text{S}:\text{Tb}$ ,  $\text{Y}_2\text{O}_2\text{S}:\text{Eu}$ , and  $\text{Y}_2\text{O}_3:\text{Eu}$ ) with mean grain size of  $7 \mu\text{m}$ , were used. The layers had various coating weights from 20 to  $140 \text{ mg/cm}^2$ .
2. The layers were irradiated with X-rays from a medical X-ray unit with various X-ray tube voltages. The beam was filtered by 20 mm of aluminum to simulate attenuation by patient's body.
3. The light emitted by the irradiated layers was measured by a photomultiplier (EMI 9558 QB) connected to an electrometer (Cary 401). These measurements represent light energy flux so they had to be converted into optical quantum fluence  $\Phi_\lambda$  in Eq. (9). For this, energy fluence data were divided by the mean energy of one optical quantum ( $\overline{\hbar\omega}$ )
4. The mean energy ( $\overline{\hbar\omega}$ ) of optical quanta was determined from emission spectrum measure-

ments performed by an Oriel 7440 grating monochromator, using relation (3c).

5. The incident X-ray quantum fluence (the integral in denominator of Eq. (9)) was determined from X-ray exposure measurements performed by a PTW dosimeter (ionizing chamber type No. 23333). Exposure data were converted into quantum fluence data using the appropriate conversion factor [18].

### 2.2.2. Determination of intrinsic parameters

The intrinsic parameters  $\mu$ ,  $\sigma$ ,  $\tau$ ,  $\rho$ ,  $\eta_C$  were found as follows:

1.  $\mu$  was calculated from data on X-ray attenuation coefficients of the chemical elements Gd, Y, O, S as tabulated by Storm and Israel [14].
2.  $\eta_C$  and  $\sigma$  were determined by fitting relation (8) to the experimental data on  $G_D$ . Fitting was accomplished using the Levenberg–Marquard method [19]. The latter requires initial values for  $\eta_C$  and  $\sigma$  which were selected as follows: Regarding  $\eta_C$ , an initial estimate was determined by considering the following: (i) the intrinsic conversion efficiency values found under cathodoluminescent efficiency measurements [20]. It has been shown [21,22] that these values are very close to  $\eta_C$  found under X-ray excitation conditions; (ii)  $\eta_C$  values are inversely proportional to the fundamental electronic energy bandgap ( $E_g$ ) of the material [20]. Thus,  $Y_2O_3:Eu$  ( $E_g = 5.6$  eV) was expected to exhibit lower intrinsic conversion efficiency than  $Y_2O_2S:Eu$  ( $E_g = 4.6$  eV); (iii) terbium-activated phosphors are shown to exhibit higher intrinsic conversion efficiency than europium-activated ones [20]; (iv)  $\eta_C$  values published in the literature mainly are for  $Y_2O_2S:Tb$  and  $La_2O_2S:Tb$  phosphors [21,22]. Regarding the initial value of  $\sigma$ , it was determined by allowing  $\sigma$  to vary interactively until a satisfactory visual coincidence between experimental and calculated curves was achieved. The effect of K-characteristic radiation generation was also taken into account as explicitly described in a previous study [10]. Finally, the initial estimates of  $\eta_C$  and  $\sigma$  were used as inputs to the Levenberg–Marquard algorithm for best fitting. The  $\eta_C$  and  $\sigma$  final values, corre-

sponding to best curve coincidence, were then adopted as the values expressing the light generation and light attenuation properties of the phosphor material.

3.  $\beta$  in Eq. (7d) or,  $\tau$  and  $\rho$  were found via reflectivity measurements, performed in order to obtain the values of  $r_0, r_1$  and  $R_\infty$  and then  $\tau$  and  $\rho$  by relations (7) [11,12]. Reflectivities were found not to differ among the various phosphors measured. Thus,  $\beta$  and  $\rho$  were considered to be approximately equal for all phosphors and  $\tau$  was directly proportional to  $\sigma$ .

## 3. Results and discussion

Fig. 1 shows the variation of detector optical gain with phosphor coating weight for the phosphors considered. Points represent experimental data while solid lines are curves obtained by fitting Eq. (8), considering  $u = 0$ , to the experimental points. The shape of the curves may be explained by considering the variation of quantum detection efficiency ( $\eta_Q$ ) and light transmission efficiency ( $g_\lambda$ ) with phosphor layer thickness.  $\eta_Q$ , which expresses the absorption of X-ray quanta, augments exponentially with increasing phosphor thickness. This means that  $\eta_Q$  should tend towards a saturation value at relatively thick layers, remaining approximately constant as thickness increases thereafter.  $g_\lambda$ , which expresses the probability of optical photon escape from the phosphor mass, decreases with the increasing probability of optical absorption and optical scattering, which in turn increase with phosphor thickness. Thus, the shape of the DOG curves shows two distinct parts: an increasing part corresponding to low and medium coating weights, which is mainly determined by  $\eta_Q$  and a slightly decreasing part, at thicker coating weights, which is principally affected by  $g_\lambda$ .

The height of each curve is affected by the following three factors:

1. The number  $m_0$  of optical photons produced within the phosphor, which is determined by the intrinsic X-ray to light conversion efficiency ( $\eta_C$ ) of the corresponding phosphor material. This efficiency, which increases light output, depends on the type of ion activator, on the energy of the

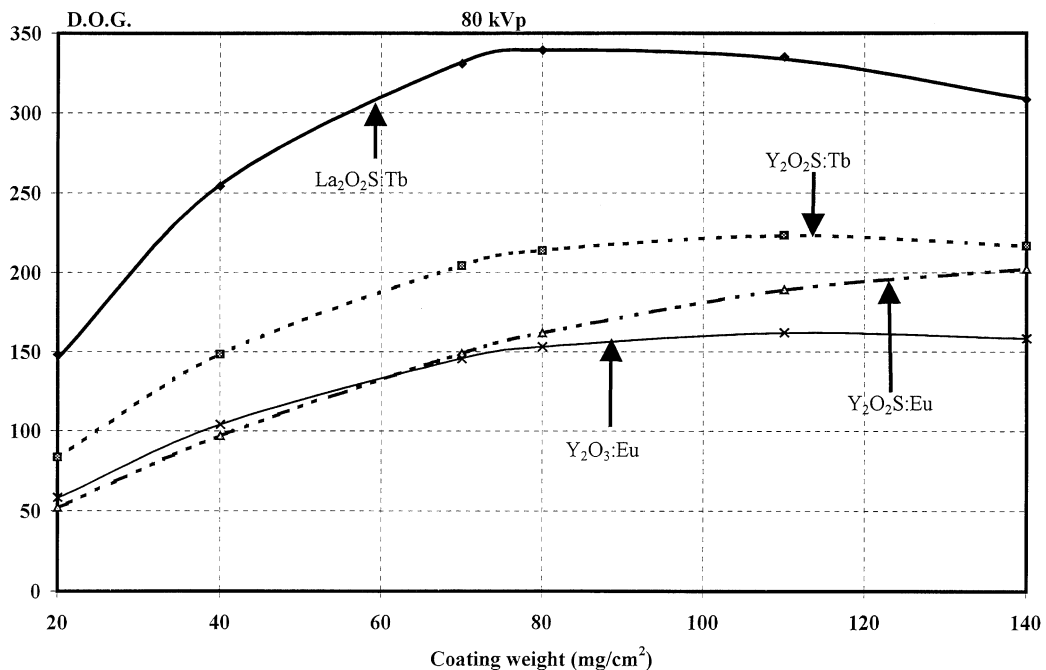


Fig. 1. Variation of detector optical gain (DOG) with coating weight for  $\text{La}_2\text{O}_2\text{S:Tb}$ ,  $\text{Y}_2\text{O}_2\text{S:Tb}$ ,  $\text{Y}_2\text{O}_2\text{S:Eu}$ , and  $\text{Y}_2\text{O}_3:\text{Eu}$  phosphor materials.

Table 1  
Values of intrinsic parameters  $\sigma$  and  $\eta_c$  of the three phosphors used

	$\text{La}_2\text{O}_2\text{S:Tb}$	$\text{Y}_2\text{O}_2\text{S:Tb}$	$\text{Y}_2\text{O}_2\text{S:Eu}$	$\text{Y}_2\text{O}_3:\text{Eu}$
Intrinsic X-ray to light conversion efficiency ( $\eta_c$ )	0.18	0.18	0.11	0.095
Reciprocal diffusion length $\sigma$ ( $\text{cm}^2/\text{g}$ )	30	30	15	23

fundamental energy bandgap of the material, on the crystal site symmetry etc. Table 1 shows the conversion efficiencies for various phosphors considered in this study. Terbium-activated materials exhibit higher values than the corresponding europium-activated materials.

2. The X-ray absorption coefficient  $\mu(E)$ , which increases optical photon production, is a function of the X-ray energy and of the effective atomic number and density of the material.  $\text{La}_2\text{O}_2\text{S}$ , having higher density and effective atomic number than  $\text{Y}_2\text{O}_2\text{S}$  and  $\text{Y}_2\text{O}_3$ , was also found to have higher  $\mu(E)$  values.

3. The optical attenuation properties of the phosphor, which may be expressed by the coefficient  $\sigma$ . This coefficient depends on the emitted light wavelength and on the size of the phosphor particles (grains) and causes reduction in the light output. Table 1 shows the values of  $\sigma$  for the phosphors considered, which were determined using the fitting technique on the experimental DOG data. As it is observed, the europium activated material exhibited lower  $\sigma$  values than the terbium activated ones. This difference may be explained by considering the fact that the europium activator induces the

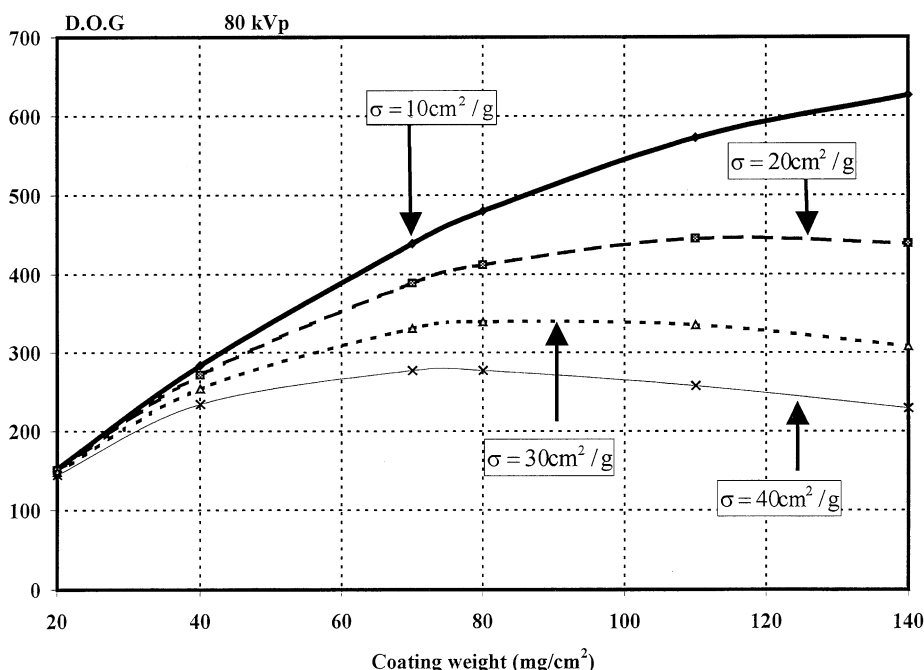


Fig. 2. Variation of detector optical gain (DOG) with coating weight for different values of optical attenuation ( $\sigma$ ).

emission of reddish light, which is of longer wavelength than the green light emitted by the terbium phosphors. Green light is easily attenuated within the layer resulting in higher values of  $\sigma$ .

To simulate the effect of  $\sigma$  and  $\eta_C$  parameters on the DOG curves, Figs. 2 and 3 were obtained considering  $\text{La}_2\text{O}_2\text{S}$  phosphor material and that all phosphor parameters were kept constant allowing  $\sigma$  to vary in Fig. 2 and  $\eta_C$  in Fig. 3. As it is shown, DOG decreases with increasing optical attenuation ( $\sigma$ ) and increases with increasing X-ray to light conversion efficiency ( $\eta_C$ ).

Fig. 4 shows four MTF curves of  $\text{La}_2\text{O}_2\text{S}$  phosphor, calculated according to relation (9). Each curve corresponds to different  $\sigma$  value,  $\sigma$  ranging between 10 and  $40 \text{ cm}^2/\text{g}$ . This was done in order to study the effect of the phosphor's optical attenuation properties on MTF and hence, on spatial resolution and image contrast characterizing the produced image. As it is observed, MTF values decrease with decreasing  $\sigma$ , which is in contradic-

tion to what was observed in the case of DOG (see Fig. 2). However, in the case of a material with high optical attenuation coefficient (e.g.  $\text{La}_2\text{O}_2\text{S}$ ), what should principally be attenuated are laterally directed optical quanta since they travel longer distances to escape the phosphor than quanta directed vertically towards the emitting surface. Thus, light produced after the absorption of an X-ray quantum within a phosphor with high  $\sigma$ , spreads over a smaller area at the emitting surface. This should result in narrow PSF giving higher MTF values, which is in accordance with the calculated curves shown in Fig. 4. These results may be of value when spectral matching between the light emitted by the phosphor and the spectral sensitivity of the optical detector (film, photocathode, photodiode etc.) is considered. For a given type of optical detector, the phosphor's activator, which affects the emitted optical spectrum, should be suitably selected so that the wavelength of the emitted light matches the sensitivity of the optical detector. However, light wavelength affects significantly the optical attenuation properties of the phosphor (value of  $\sigma$ ), which,

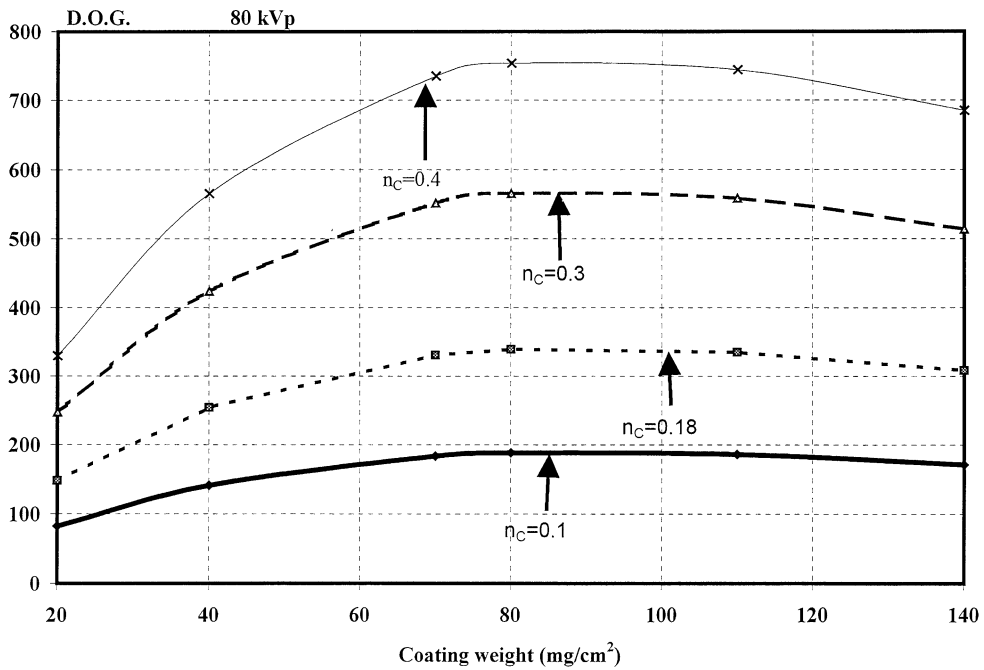


Fig. 3. Variation of detector optical gain (DOG) with coating weight for different values of X-ray to light conversion efficiency ( $\eta_c$ ).

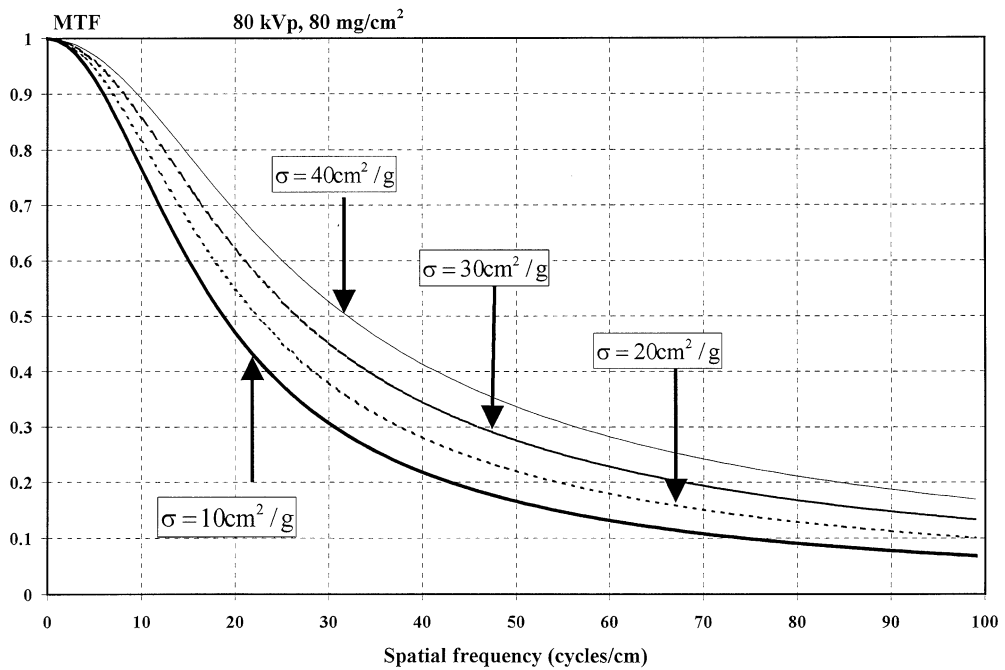


Fig. 4. Variation of modulation transfer function (MTF) with frequency for different values of optical attenuation ( $\sigma$ ).

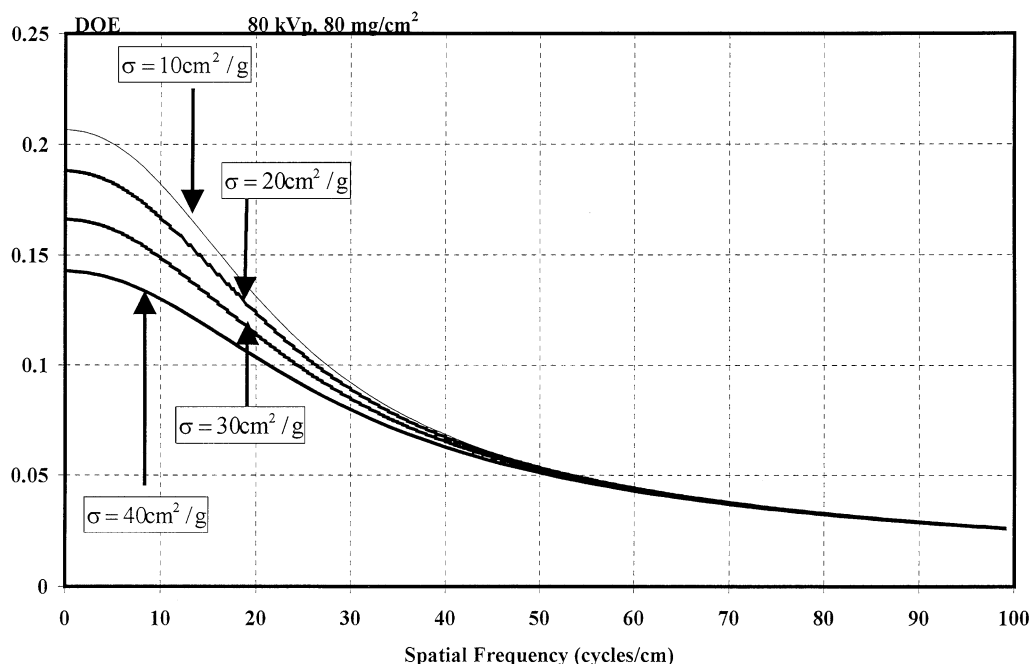


Fig. 5. Variation of detective quantum efficiency (DQE) with frequency for different values of optical attenuation ( $\sigma$ ).

in turn, affect the MTF values. Thus, spectral matching optimization, although it increases image brightness may cause an inverse effect on MTF and hence, spatial resolution and contrast may be degraded.

Fig. 5 shows DQE curves calculated by relation (14) corresponding to the four  $\sigma$  values used in DOG and MTF calculation. As it is observed, DQE increases when the phosphor exhibits low optical attenuation properties (low  $\sigma$ ) but the rate of decrease depends on the spatial frequency. For frequencies higher than 60lp/mm the four curves coincide showing that at higher frequencies the role of  $\sigma$  on the signal-to-noise ratio is insignificant. This behavior may be principally attributed to the combined effects of the zero-frequency DOG, which increases with decreasing  $\sigma$  (see Fig. 2), and MTF, which increases with increasing  $\sigma$ . At very low frequencies, differences between the MTF curves tend to be eliminated, since all MTF values tend towards  $MTF = 1$ . Thus, optical gain differences due to various  $\sigma$  values are more apparent and their effect on DQE variation is more significant. As spatial frequency increases, the MTF

curves calculated with low  $\sigma$  values decrease with frequency more rapidly than the MTFs corresponding to high  $\sigma$ , while zero-frequency DOG remains constant. Thus, the differences between the curves are eliminated for frequencies higher than 60lp/cm. These results may also be taken into account in cases where the emitted light wavelength, which influences the value of  $\sigma$ , should be suitably selected in order to optimize spectral matching. However, in contrast to MTF, DQE and hence SNR decrease with increasing optical attenuation properties of the phosphor.

MTF and DQE curves were also similarly calculated by varying the value of the intrinsic X-ray to light conversion efficiency ( $\eta_C$ ). Results showed that, in contrast to DOG, both MTF and DQE curves remained unaltered for various  $\eta_C$  values ranging from 0.10 to 0.40. This may be explained by considering that MTF is, by definition, the ratio of the emitted optical fluence to the zero-frequency-emitted optical fluence (see relation 10), which are both functions of  $\eta_C$ . Similarly, in the case of DQE both output signal and quantum noise depend on  $\eta_C$ .

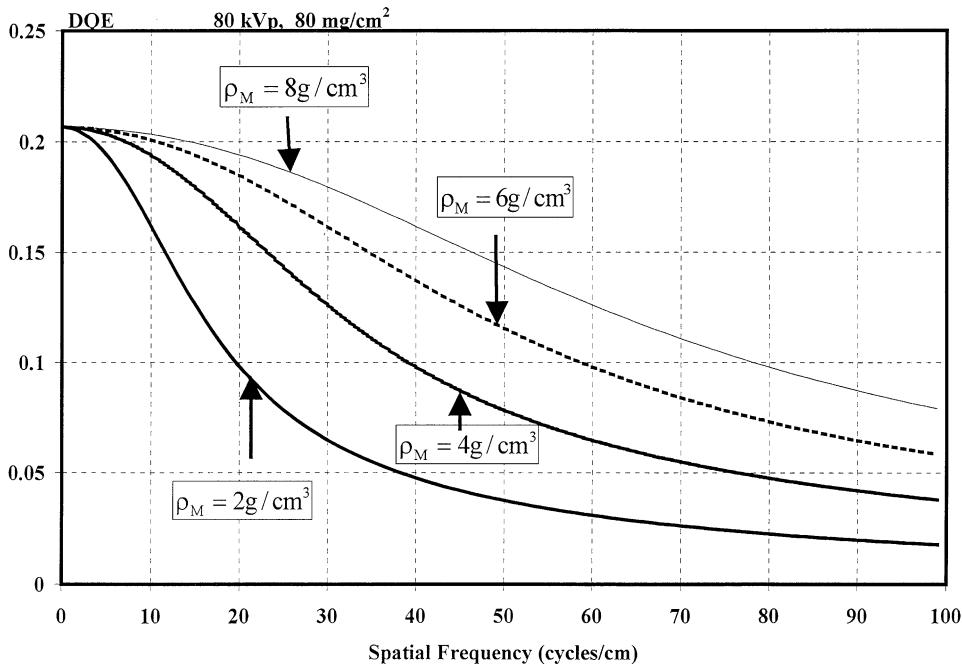


Fig. 6. Variation of detective quantum efficiency (DQE) with frequency for different values of material density.

Fig. 6 shows four DQE curves corresponding to the hypothetical case that all the physical properties and parameters of a phosphor material remain unaltered except for the material density. Curves were calculated by allowing density values to vary from  $2 \text{ g/cm}^2$  to  $8 \text{ g/cm}^2$ . As it is observed, a high-density material shows improved signal-to-noise ratio characteristics as compared to a low-density phosphor. These results may also be qualitatively explained by considering that for a given coating weight value, the thickness (in  $\mu\text{m}$ ) of a high-density layer is lower. Thus, light spread is limited in a small area on the phosphor's emitting surface giving narrow PSF and hence higher MTF values. This was also verified by calculating MTF for the same density values. The corresponding MTF curves are not shown since they were very similar to the DQE curves.

### Acknowledgements

This study is dedicated to the memory of Prof. G.E. Giakoumakis, leading member of our

team, whose work on phosphor materials has inspired us to continue.

### References

- [1] I. Kandarakis, D. Cavouras, E. Kanellopoulos, G.S. Panayiotakis, C.D. Nomicos, Nucl. Instr. and Meth. A 417 (1998) 86.
- [2] I. Kandarakis, D. Cavouras, P. Prassopoulos, E. Kanellopoulos, C.D. Nomicos, G.S. Panayiotakis, Appl. Phys. A 67 (1998) 521.
- [3] R. Van Metter, Med. Phys. 19 (1992) 53.
- [4] R.K. Swank, Appl. Opt. 12 (1973) 1865.
- [5] ICRU, Modulation transfer function of screen-film systems, ICRU Report 41, 1986.
- [6] P.C. Bunch, K.E. Huff, R. Van Metter, J. Opt. Soc. Am. A4 (1987) 902.
- [7] M. Rabbani, R. Shaw, R. Van Metter, J. Opt. Soc. Am. A4 (1987) 895.
- [8] I. Kandarakis, D. Cavouras, G.S. Panayiotakis, D. Triantis, C.D. Nomicos, Nucl. Instr. and Meth. A 399 (1997) 335.
- [9] G. Lubberts, J. Opt. Soc. Am. 58 (1968) 1475.
- [10] N. Kalivas, I. Kandarakis, D. Cavouras, L. Costaridou, C.D. Nomicos, G.S. Panayiotakis, Nucl. Instr. and Meth. A. 430 (1999) 559.

- [11] G.W. Ludwig, *J. Electrochem. Soc.* 118 (1971) 1152.
- [12] D. Cavouras, I. Kandarakis, G. Panayiotakis, E.K. Evangelou, C.D. Nomicos, *Med. Phys.* 23 (1996) 1965.
- [13] D.M. Tucker, G.T. Barnes, D.B. Chakraborty, *Med. Phys.* 18 (1991) 211.
- [14] E. Storm, H. Israel, Report LA-3753, Los Alamos Scientific Laboratory, University of California, 1967.
- [15] I. Kandarakis, D. Cavouras, C.D. Nomicos, G.S. Panayiotakis, *Appl. Phys. B.* 68 (1999) 1121.
- [16] R. Shaw, R. Van Metter, *Proc. SPIE* 454 (1984) 128.
- [17] D. Cavouras, I. Kandarakis, M. Kanellopoulos, C.D. Nomicos, G.S. Panayiotakis, *Appl. Radiat. Isot.* 51 (1999) 59.
- [18] W.R. Hendee, *Medical Radiation Physics*, Year Book Medical Publishers, Chicago, 1970, pp. 145–148.
- [19] W.H. Press, B.P. Flannery, S.A. Teukolsky, W.T. Vetterling, in: *Numerical Recipes in C: The Art of Scientific Computing*, Cambridge University Press, Cambridge, 1990, pp. 542–547.
- [20] R.C. Alig, S. Bloom, *J. Electrochem. Soc.* 124 (1977) 1136.
- [21] J.A. de Poorter, A. Bril, *J. Electrochem. Soc.* 122 (1975) 1086.
- [22] B.A. Arnold, in: A.G. Haus (Ed.), *The Physics of Medical Imaging: Recording System, Measurements and Techniques*, American Association of Physicists in Medicine, New York, 1979, pp. 30–71.